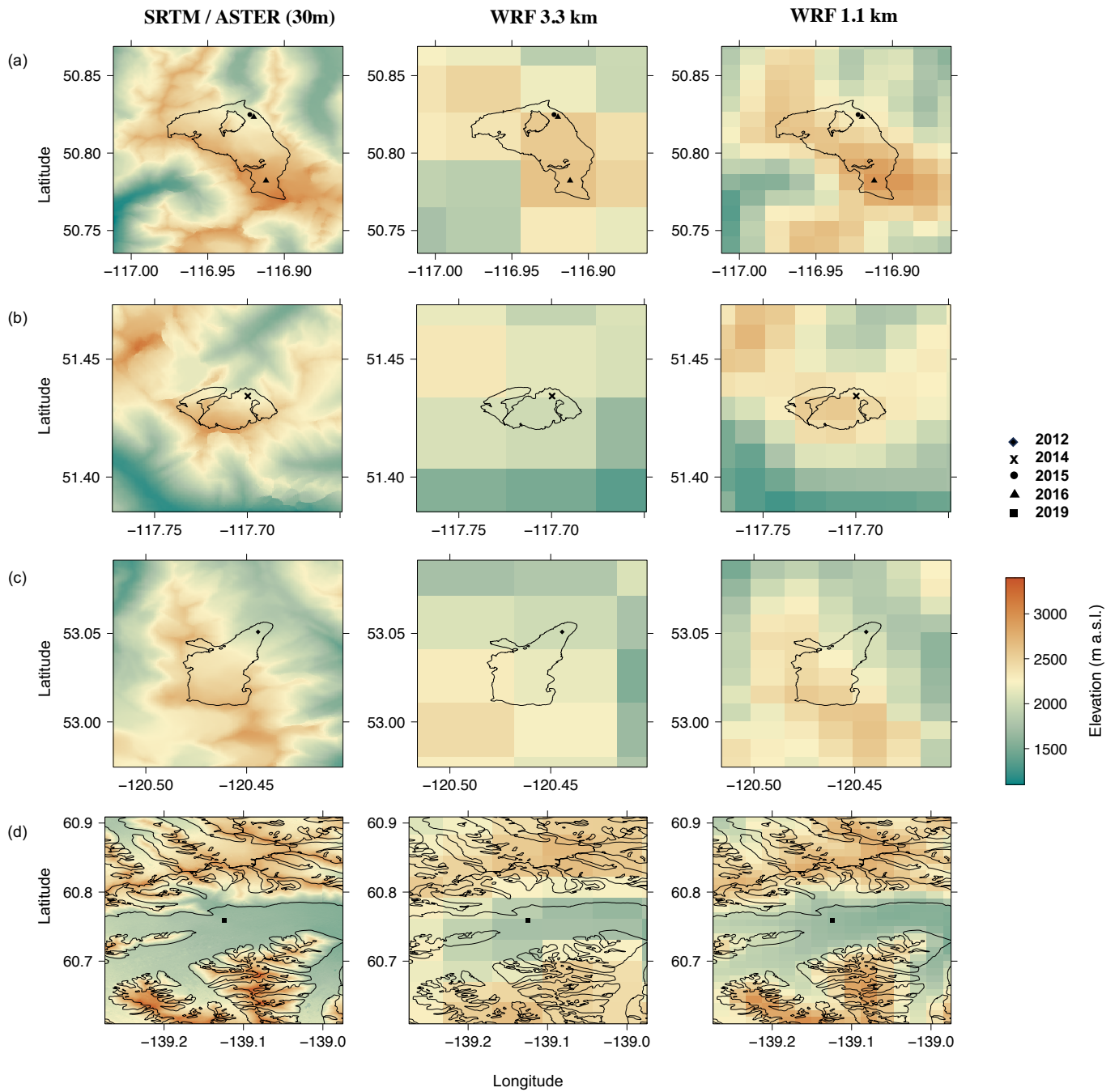
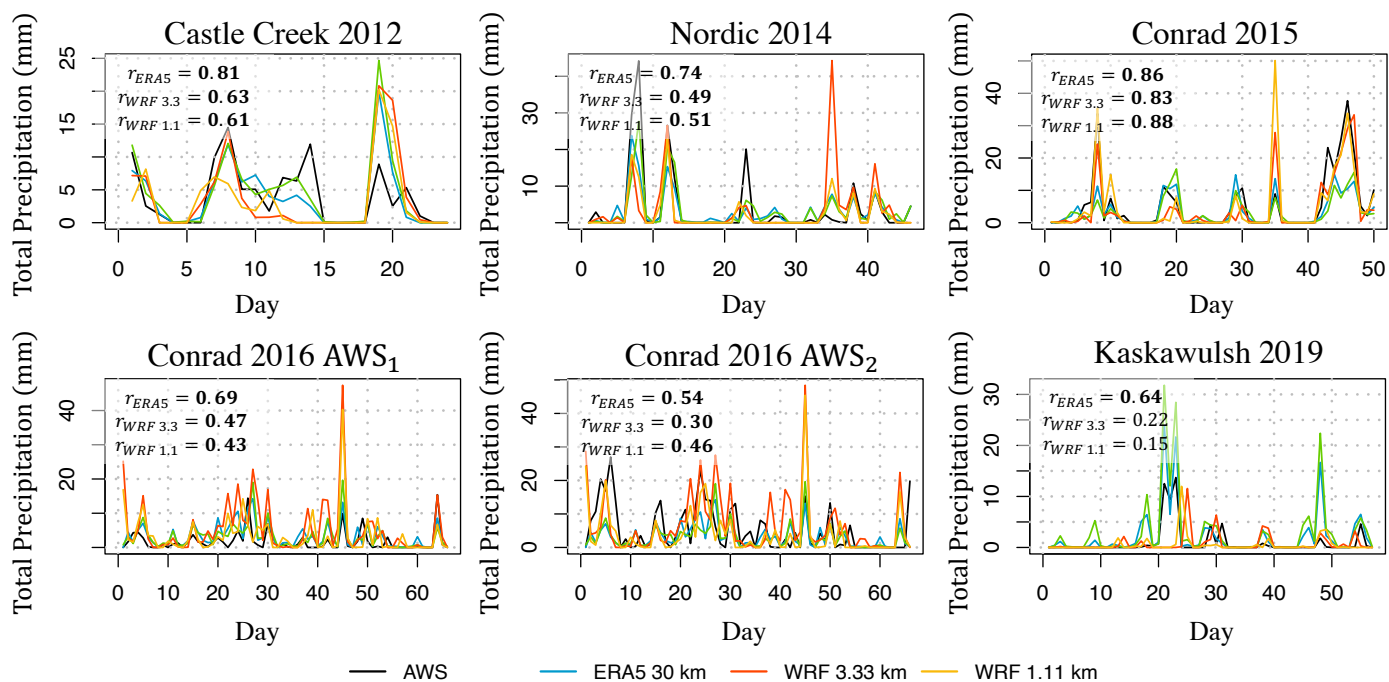


Supplementary Figures

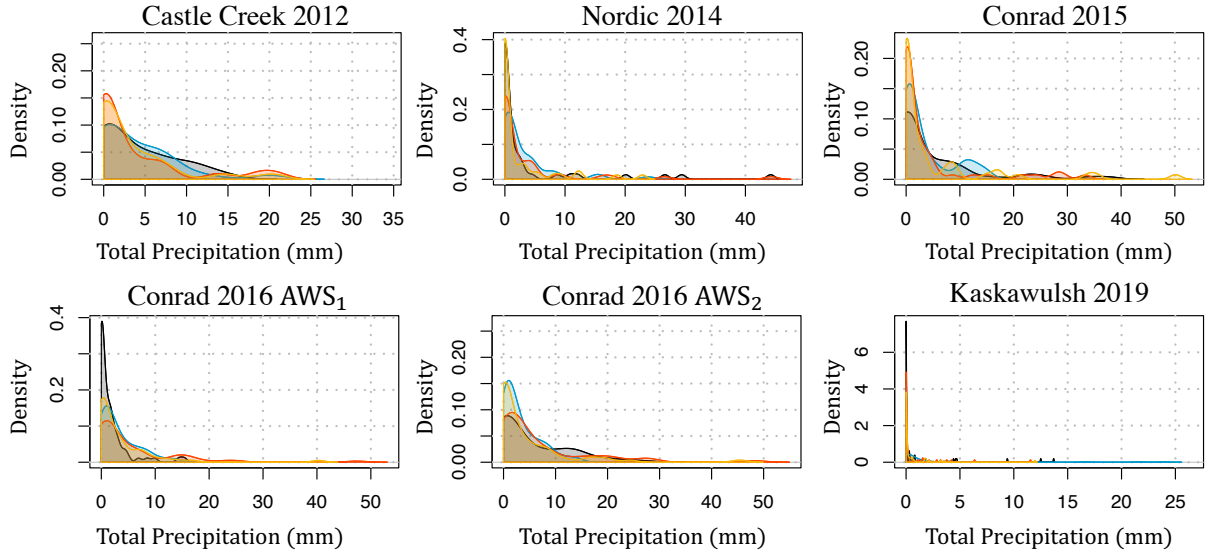


**Figure S1:** Topography for the domain covering (a) Conrad, (b) Nordic and (c) Castle Creek and (d) Kaskawulsh glaciers from a high-resolution DEM at 30 m grid spacing in comparison to the topography from WRF at 3.3 km and 1.1 km grid spacing. DEM data from SRTM (NASA JPL, 2013; Farr et al., 2007) were used for Castle Creek, Nordic and Conrad glaciers, and ASTER (ASTER, 2019; Abrams et al., 2020) for Kaskawulsh glacier. Markers indicate the AWS sites in different years. The outlines of the glaciers (black lines) are taken from the Randolph Glacier Inventory (RGI V6; RGI Consortium, 2017). Only on the map with Kaskawulsh glacier the neighboring glaciers are also shown.

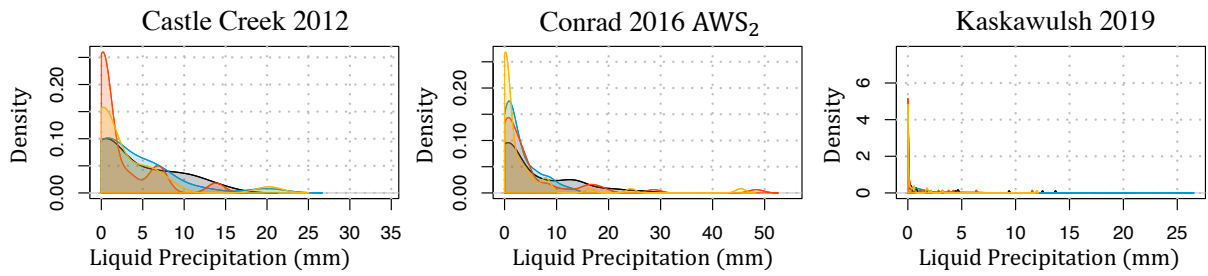


**Figure S2:** Modeled (ERA5, WRF at 3.3 km and WRF at 1.1 km) and observed (AWS data) timeseries of daily total precipitation over the observational period at each site. Bold values of correlation coefficient,  $r_{sp}$ , indicate a statistically significant correlation at the 5% confidence level. WRF is run with the REF configuration.

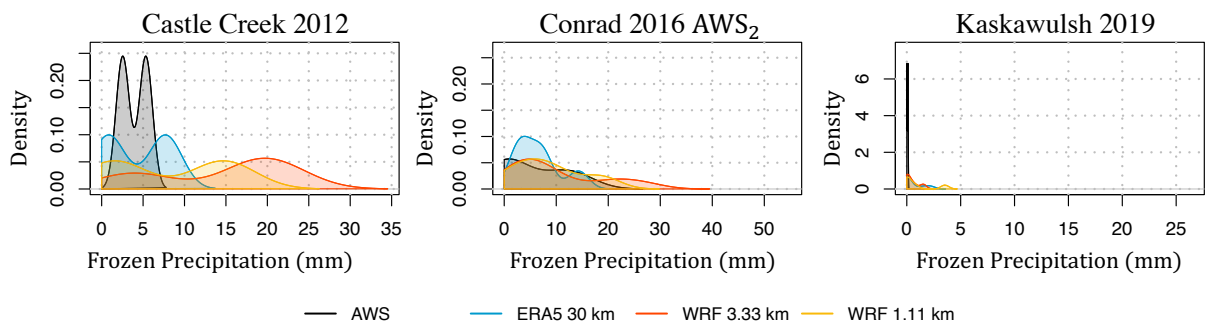
**(a) Density of Total Precipitation**



**(b) Density of Rainfall**



**(c) Density of Snowfall**



— AWS      — ERA5 30 km      — WRF 3.33 km      — WRF 1.11 km

**Figure S3:** Modeled (ERA5, ERA5-Land, WRF at 3.3km and WRF at 1.1km) and observed (AWS data) densities of (a) total, (b) liquid and (c) frozen daily precipitation over the observational period. We differentiate between liquid and frozen precipitation using a temperature threshold of 0°C. The densities of liquid and frozen precipitation are displayed only if there were days with snowfall during the observational period. WRF is run with REF configuration.

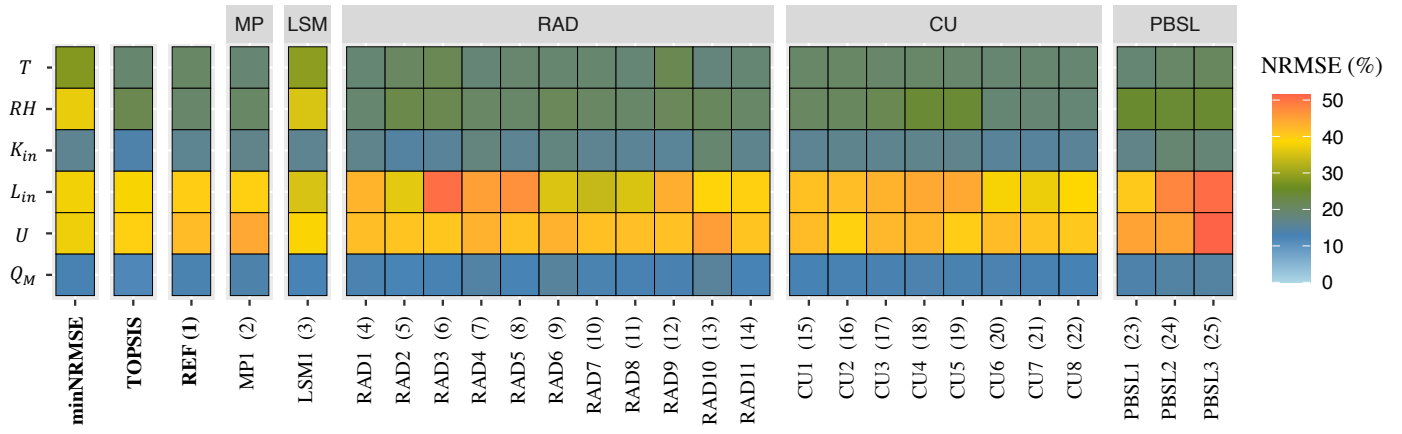


**Figure S4:** Visual representation of NRMSE calculated from the multiple 6-day WRF runs with three different configurations (minNRMSE, TOPSIS, REF) and the configurations used in the sensitivity runs (enumerated in brackets) with labels corresponding to their parameterization category with scheme that differs from REF. For full names of parameterization categories see Table S2. The NRMSE is calculated for each of the following variables: air temperature ( $T$ ), relative humidity ( $RH$ ), incoming shortwave ( $K_{in}$ ) and longwave ( $L_{in}$ ) radiation, wind speed ( $U$ ) and total melt energy ( $Q_M$ ).

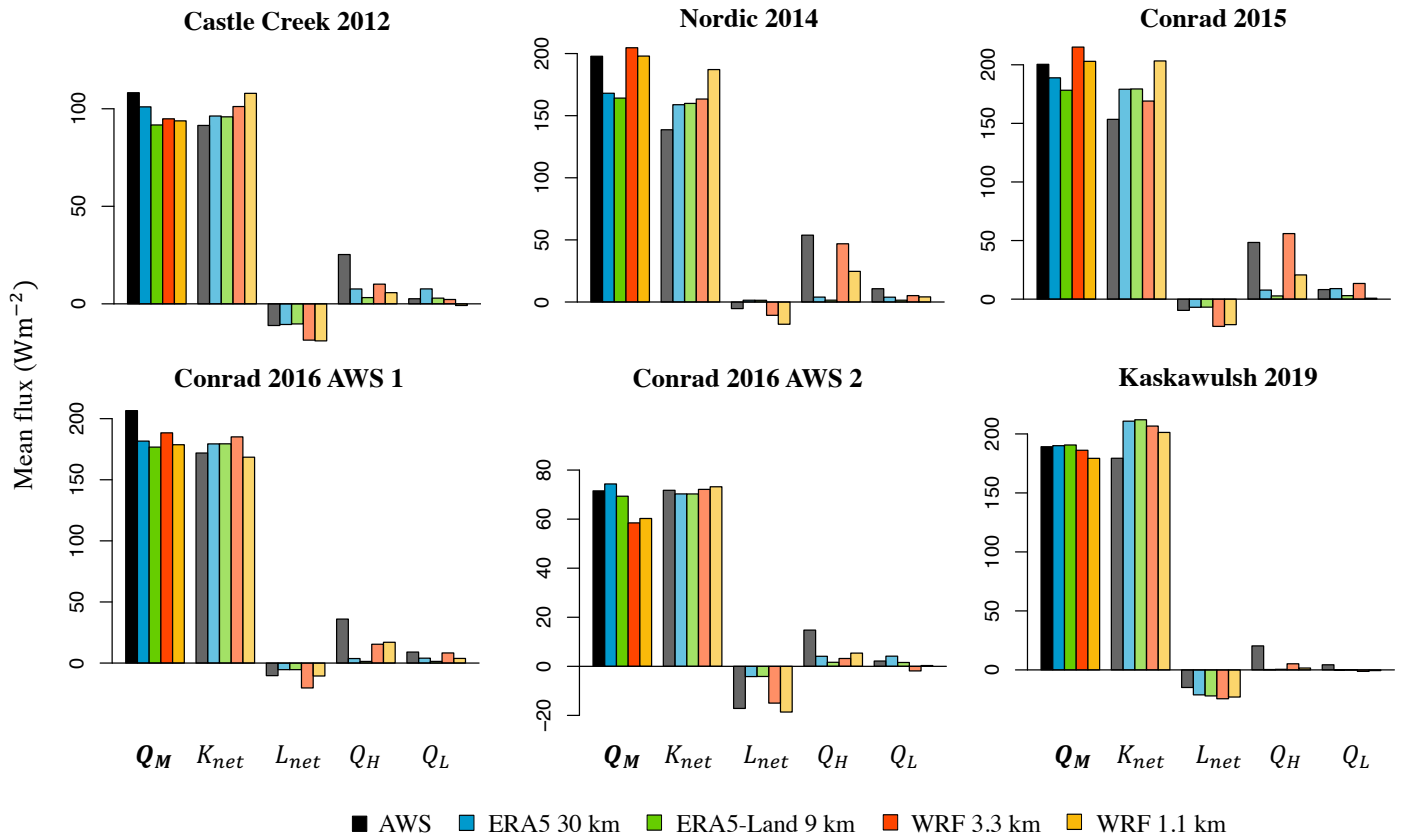


**Figure S5:** Mean daily total of melt energy ( $Q_M$ ), as averaged over the observational period at each site, and the mean daily SEB components, including net shortwave ( $K_{net}$ ) and longwave ( $L_{net}$ ) radiation, sensible ( $Q_H$ ) and latent ( $Q_L$ ) heat fluxes, per glacier site using data from observations (AWS), ERA5 at 30 km grid spacing, ERA5-Land at 9 km, WRF at 3.3 km and WRF at 1.1 km. The REF configuration is used in the WRF runs. For this figure, only hourly values with  $Q_M > 0$  are used in the calculation of mean daily fluxes.

## Supplementary Tables

**Table S1:** Elevation for each study site (in meter above sea level) derived from AWS (on-site GPS), ERA5 at 30 km grid spacing, ERA5-Land at 9 km, WRF at 3.3 km and 1.1 km, and a high-resolution DEM at 30 m grid spacing: SRTM ([NASA JPL, 2013](#); [Farr et al., 2007](#)) for Castle Creek, Nordic and Conrad glaciers, and ASTER ([ASTER, 2019](#); [Abrams et al., 2020](#)) for Kaskawulsh glacier). Numbers in brackets show the respective difference to the AWS elevation.

Glacier site	AWS	ERA5	ERA5-Land	WRF 3.3 km	WRF 1.1 km	SRTM / ASTER
Castle Creek 2012	<b>1967</b>	1762 (-205)	1987 (+20)	2157 (+190)	1915 (-52)	1977 (+10)
Nordic 2014	<b>2208</b>	1785 (-423)	1866 (-342)	2124 (-84)	2298 (+90)	2203 (-5)
Conrad 2015	<b>2138</b>	1901 (-237)	2145 (+7)	2412 (+274)	2184 (+46)	2163 (+25)
Conrad 2016 AWS <sub>1</sub>	<b>2164</b>	1901 (-263)	2145 (-19)	2567 (+403)	2217 (+53)	2182 (+18)
Conrad 2016 AWS <sub>2</sub>	<b>2909</b>	1901 (-1008)	2145 (-764)	2618 (-291)	2944 (+35)	2910 (+1)
Kaskawulsh 2019	<b>1666</b>	2122 (+456)	2159 (+493)	1709 (+43)	1659 (-7)	1709 (+43)

**Table S2:** Summary of WRF configurations with physics parameterization schemes used in the 25 sensitivity runs. Radiation schemes (RAD) are split into longwave (LW) and shortwave (SW) schemes. The choice of planetary boundary (PBL) and surface layer (SL) schemes is interdependent, and therefore aggregated into one PBSL category. In the parameterization for the cumulus process (CU), the on/off label in brackets refers to the parameterization being switched 'on' or 'off' in each of the WRF domains  $d_1$  (30 km) –  $d_2$  (10 km) –  $d_3$  (3.3 km) –  $d_4$  (1.1 km). For each of the sensitivity runs, only one physics parameterization scheme is changed at a time, and all other specifications are the same as for the reference (REF) configuration (Table 3).

Microphysics (MP)		Cumulus (CU)	
MP1	Morrison 2-Moment <sup>a</sup>	CU1	Grell 3D Ensemble <sup>h</sup> (on – on – on – off)
Land Surface Model (LSM)		CU2	Grell 3D Ensemble (on – on – on – on)
LSM1	Unified Noah <sup>b</sup>	CU3	Kain–Fritsch <sup>i</sup> (on – on – off – off)
Radiation (RAD)		CU4	Kain–Fritsch (on – on – on – off)
RAD1	LW/SW: CAM <sup>c</sup>	CU5	Kain–Fritsch (on – on – on – on)
RAD2	LW: RRTM <sup>d</sup> , SW: Dudhia <sup>e</sup>	CU6	Betts–Miller–Janjic <sup>j</sup> (on – on – off – off)
RAD3	LW: CAM, SW: Dudhia	CU7	Betts–Miller–Janjic (on – on – on – off)
RAD4	LW: CAM, SW: Goddard <sup>f</sup>	CU8	Betts–Miller–Janjic (on – on – on – on)
RAD5	LW: CAM, SW: RRTMG <sup>g</sup>	Planetary Bound./Surface Layer (PBSL)	
RAD6	LW: RRTM, SW: Goddard	PBSL1	PBL: MYNN <sup>k</sup> Level 2.5 SL: MYNN
RAD7	LW: RRTM, SW: CAM	PBSL2	PBL: Yonsei University <sup>l</sup> SL: Revised MM5 <sup>m</sup>
RAD8	LW: RRTM, SW: RRTMG	PBSL3	PBL: Mellor–Yamada–Janjic (MYJ) <sup>n</sup> SL: Eta Similarity <sup>o</sup>
RAD9	LW: RRTMG. SW: Dudhia		
RAD10	LW: RRTMG. SW: Goddard		
RAD11	LW: RRTMG, SW: CAM		

<sup>a</sup> Morrison et al. (2009)  
<sup>b</sup> Tewari et al. (2004)  
<sup>c</sup> Collins et al. (2004)  
<sup>d</sup> Mlawer et al. (1997)  
<sup>e</sup> Dudhia (1989)  
<sup>f</sup> Max and Suarez (1994); Matsui et al. (2018)  
<sup>g</sup> Iacono et al. (2008)  
<sup>h</sup> Grell (1993); Grell and Dévényi (2002)  
<sup>i</sup> Kain (2004); The Kain-Fritsch trigger option was set to default.  
<sup>j</sup> Janjić (1994)  
<sup>k</sup> Nakanishi and Niino (2006, 2009); Olson et al. (2019)  
<sup>l</sup> Hong et al. (2006)  
<sup>m</sup> Jiménez et al. (2012)  
<sup>n</sup> Janjić (1994); Mesinger (1993)  
<sup>o</sup> Monin and Obukhov (1954); Janjić (1994, 1996, 2002)

**Table S3:** EC-derived roughness lengths [m] for momentum ( $z_{0v}$ ), temperature ( $z_{0T}$ ) and humidity ( $z_{0q}$ ) used in the calculations of sensible and latent heat fluxes at each study site.

Site	$z_{0v}$	$z_{0T}$	$z_{0q}$
Castle Creek 2012	$10^{-2.5}$	$10^{-4.5}$	$10^{-4.0}$
Nordic 2014	$10^{-2.5}$	$10^{-5.0}$	$10^{-6.0}$
Conrad 2015	$10^{-2.5}$	$10^{-4.0}$	$10^{-3.5}$
Conrad 2016 AWS <sub>1</sub>	$10^{-3.0}$	$10^{-4.5}$	$10^{-4.5}$
Conrad 2016 AWS <sub>2</sub>	$10^{-2.5}$	$10^{-5.0}$	$10^{-5.0}$
Kaskawulsh 2019	$10^{-3.1}$	$10^{-5.9}$	$10^{-5.9}$

**Table S4:** Model performance, evaluated by  $r_{sp}$  and NNSE, over the whole observational period in simulating daily air temperature ( $T$ ), relative humidity ( $RH$ ), total precipitation ( $P$ ), wind speed ( $U$ ), incoming shortwave ( $K_{in}$ ) and longwave ( $L_{in}$ ) radiation, sensible ( $Q_H$ ) and latent ( $Q_L$ ) heat fluxes and total melt energy ( $Q_M$ ). The melt energy is estimated according to the SEB model (Eq. 1). The WRF runs are based on three configurations of physics parameterizations: REF, minNRMSE and TOPSIS. The model performance is shown as the mean ( $\pm$  one standard deviation) across the six study sites, with equal weighing of each site. Values in bold highlight the best performing model for the given variable. Values in purple highlight a statistically significant correlation at the 5% confidence level for at least four of the six glacier sites.

Variable	ERA5	ERA5-Land	REF	WRF 3.3 km		REF	WRF 1.1 km	
	30 km	9 km		minNRMSE	TOPSIS		TOPSIS	minNRMSE
$r_{sp}$								
<b>T</b>	<b>0.86</b> $\pm$ 0.19	<b>0.89</b> $\pm$ 0.14	<b>0.89</b> $\pm$ 0.05	<b>0.86</b> $\pm$ 0.04	<b>0.88</b> $\pm$ 0.03	<b>0.91</b> $\pm$ 0.03	<b>0.88</b> $\pm$ 0.03	<b>0.90</b> $\pm$ 0.01
<b>RH</b>	<b>0.74</b> $\pm$ 0.20	<b>0.75</b> $\pm$ 0.15	<b>0.70</b> $\pm$ 0.21	<b>0.55</b> $\pm$ 0.19	<b>0.72</b> $\pm$ 0.19	<b>0.71</b> $\pm$ 0.20	<b>0.53</b> $\pm$ 0.25	<b>0.71</b> $\pm$ 0.17
<b>P</b>	<b>0.71</b> $\pm$ 0.11	<b>0.71</b> $\pm$ 0.11	<b>0.49</b> $\pm$ 0.22	<b>0.44</b> $\pm$ 0.28	<b>0.55</b> $\pm$ 0.21	<b>0.51</b> $\pm$ 0.24	<b>0.53</b> $\pm$ 0.24	<b>0.49</b> $\pm$ 0.26
<b>U</b>	<b>0.19</b> $\pm$ 0.36	0.13 $\pm$ 0.32	0.15 $\pm$ 0.15	0.10 $\pm$ 0.16	0.16 $\pm$ 0.20	<b>0.23</b> $\pm$ 0.20	0.20 $\pm$ 0.20	0.19 $\pm$ 0.24
<b>K<sub>in</sub></b>	<b>0.80</b> $\pm$ 0.09	<b>0.80</b> $\pm$ 0.09	<b>0.60</b> $\pm$ 0.10	<b>0.58</b> $\pm$ 0.19	<b>0.56</b> $\pm$ 0.11	<b>0.52</b> $\pm$ 0.16	<b>0.55</b> $\pm$ 0.18	<b>0.47</b> $\pm$ 0.14
<b>L<sub>in</sub></b>	<b>0.79</b> $\pm$ 0.11	<b>0.78</b> $\pm$ 0.12	<b>0.62</b> $\pm$ 0.07	<b>0.56</b> $\pm$ 0.11	<b>0.41</b> $\pm$ 0.12	<b>0.54</b> $\pm$ 0.07	<b>0.54</b> $\pm$ 0.14	<b>0.35</b> $\pm$ 0.17
<b>Q<sub>H</sub></b>	<b>0.29</b> $\pm$ 0.36	0.23 $\pm$ 0.38	<b>0.54</b> $\pm$ 0.23	<b>0.47</b> $\pm$ 0.23	<b>0.50</b> $\pm$ 0.24	<b>0.47</b> $\pm$ 0.25	<b>0.49</b> $\pm$ 0.33	<b>0.40</b> $\pm$ 0.30
<b>Q<sub>L</sub></b>	0.20 $\pm$ 0.18	0.15 $\pm$ 0.22	<b>0.55</b> $\pm$ 0.14	<b>0.48</b> $\pm$ 0.19	<b>0.55</b> $\pm$ 0.17	<b>0.59</b> $\pm$ 0.12	<b>0.53</b> $\pm$ 0.14	<b>0.61</b> $\pm$ 0.10
<b>Q<sub>M</sub></b>	<b>0.86</b> $\pm$ 0.03	<b>0.86</b> $\pm$ 0.03	<b>0.71</b> $\pm$ 0.08	<b>0.73</b> $\pm$ 0.07	<b>0.69</b> $\pm$ 0.12	<b>0.76</b> $\pm$ 0.05	<b>0.75</b> $\pm$ 0.07	<b>0.74</b> $\pm$ 0.07
NNSE (%)								
<b>T</b>	58 $\pm$ 25	54 $\pm$ 24	56 $\pm$ 18	46 $\pm$ 11	55 $\pm$ 18	<b>62</b> $\pm$ 29	51 $\pm$ 11	<b>62</b> $\pm$ 29
<b>RH</b>	22 $\pm$ 10	24 $\pm$ 11	47 $\pm$ 24	30 $\pm$ 23	48 $\pm$ 23	<b>48</b> $\pm$ 24	38 $\pm$ 16	44 $\pm$ 23
<b>P</b>	<b>57</b> $\pm$ 11	52 $\pm$ 19	41 $\pm$ 20	36 $\pm$ 18	43 $\pm$ 18	45 $\pm$ 16	41 $\pm$ 15	46 $\pm$ 20
<b>U</b>	17 $\pm$ 9	14 $\pm$ 6	27 $\pm$ 7	23 $\pm$ 9	<b>28</b> $\pm$ 9	24 $\pm$ 7	23 $\pm$ 10	23 $\pm$ 7
<b>K<sub>in</sub></b>	<b>69</b> $\pm$ 9	68 $\pm$ 10	49 $\pm$ 6	44 $\pm$ 20	49 $\pm$ 13	43 $\pm$ 4	45 $\pm$ 18	47 $\pm$ 10
<b>L<sub>in</sub></b>	<b>65</b> $\pm$ 13	<b>65</b> $\pm$ 14	41 $\pm$ 10	44 $\pm$ 10	39 $\pm$ 10	39 $\pm$ 10	45 $\pm$ 10	41 $\pm$ 11
<b>Q<sub>H</sub></b>	30 $\pm$ 12	27 $\pm$ 9	39 $\pm$ 10	33 $\pm$ 9	<b>41</b> $\pm$ 10	38 $\pm$ 11	33 $\pm$ 10	37 $\pm$ 10
<b>Q<sub>L</sub></b>	42 $\pm$ 8	45 $\pm$ 10	44 $\pm$ 7	47 $\pm$ 8	41 $\pm$ 4	<b>50</b> $\pm$ 7	<b>50</b> $\pm$ 7	47 $\pm$ 5
<b>Q<sub>M</sub></b>	<b>74</b> $\pm$ 10	71 $\pm$ 9	62 $\pm$ 6	53 $\pm$ 10	56 $\pm$ 5	67 $\pm$ 5	54 $\pm$ 11	59 $\pm$ 6

**Table S5:** Model performance, evaluated by MAPE and NMBE, over the whole observational period in simulating daily air temperature ( $T$ ), relative humidity ( $RH$ ), total precipitation ( $P$ ), wind speed ( $U$ ), incoming shortwave ( $K_{in}$ ) and longwave ( $L_{in}$ ) radiation, sensible ( $Q_H$ ) and latent ( $Q_L$ ) heat fluxes and total melt energy ( $Q_M$ ). The melt energy is estimated according to the SEB model (Eq. 1). For evaluating  $P$ , only days with positive observed  $P$  have been taken into account. The WRF runs are based on three configurations of physics parameterizations: REF, minNRMSE and TOPSIS. The model performance is shown as the mean ( $\pm$  one standard deviation) across the six study sites, with equal weighing of each site. Values in bold highlight the best performing model for the given variable.

Variable	ERA5	ERA5-Land	REF	WRF 3.3 km		REF	WRF 1.1 km	
	30 km	9 km		minNRMSE	TOPSIS		minNRMSE	TOPSIS
MAPE (%)								
<b>T</b>	67 $\pm$ 60	71 $\pm$ 52	57 $\pm$ 43	67 $\pm$ 47	<b>54</b> $\pm$ 36	63 $\pm$ 53	71 $\pm$ 53	53 $\pm$ 34
<b>RH</b>	33 $\pm$ 14	31 $\pm$ 13	16 $\pm$ 5	27 $\pm$ 12	16 $\pm$ 7	<b>15</b> $\pm$ 5	20 $\pm$ 8	17 $\pm$ 6
<b>P</b>	287 $\pm$ 303	<b>278</b> $\pm$ 299	438 $\pm$ 349	547 $\pm$ 465	471 $\pm$ 382	279 $\pm$ 215	325 $\pm$ 263	437 $\pm$ 335
<b>U</b>	61 $\pm$ 10	71 $\pm$ 7	43 $\pm$ 7	48 $\pm$ 9	<b>41</b> $\pm$ 7	46 $\pm$ 13	49 $\pm$ 14	46 $\pm$ 11
<b>K<sub>in</sub></b>	<b>23</b> $\pm$ 7	<b>23</b> $\pm$ 7	37 $\pm$ 7	32 $\pm$ 7	29 $\pm$ 4	41 $\pm$ 17	31 $\pm$ 4	32 $\pm$ 7
<b>L<sub>in</sub></b>	<b>4</b> $\pm$ 2	<b>4</b> $\pm$ 3	7 $\pm$ 1	6 $\pm$ 2	7 $\pm$ 1	7 $\pm$ 2	6 $\pm$ 1	7 $\pm$ 1
<b>Q<sub>H</sub></b>	94 $\pm$ 22	98 $\pm$ 18	89 $\pm$ 28	99 $\pm$ 31	87 $\pm$ 29	81 $\pm$ 23	101 $\pm$ 30	<b>78</b> $\pm$ 25
<b>Q<sub>L</sub></b>	279 $\pm$ 227	<b>150</b> $\pm$ 76	268 $\pm$ 150	284 $\pm$ 185	255 $\pm$ 115	234 $\pm$ 191	263 $\pm$ 157	215 $\pm$ 155
<b>Q<sub>M</sub></b>	35 $\pm$ 20	<b>34</b> $\pm$ 20	48 $\pm$ 25	50 $\pm$ 26	50 $\pm$ 23	37 $\pm$ 16	51 $\pm$ 26	47 $\pm$ 27
NMBE (%)								
<b>T</b>	-9 $\pm$ 73	2 $\pm$ 69	-13 $\pm$ 42	-33 $\pm$ 50	<b>0</b> $\pm$ 46	-17 $\pm$ 48	-43 $\pm$ 43	-2 $\pm$ 37
<b>RH</b>	33 $\pm$ 14	31 $\pm$ 13	<b>-3</b> $\pm$ 14	19 $\pm$ 23	-6 $\pm$ 13	-9 $\pm$ 11	11 $\pm$ 17	-12 $\pm$ 9
<b>P</b>	235 $\pm$ 318	227 $\pm$ 317	352 $\pm$ 353	463 $\pm$ 473	368 $\pm$ 373	<b>117</b> $\pm$ 206	231 $\pm$ 263	320 $\pm$ 335
<b>U</b>	-61 $\pm$ 10	-71 $\pm$ 7	-20 $\pm$ 18	-36 $\pm$ 14	<b>-16</b> $\pm$ 20	-40 $\pm$ 16	-42 $\pm$ 13	-38 $\pm$ 15
<b>K<sub>in</sub></b>	18 $\pm$ 10	18 $\pm$ 10	20 $\pm$ 10	-14 $\pm$ 19	<b>0</b> $\pm$ 11	31 $\pm$ 24	-7 $\pm$ 21	9 $\pm$ 14
<b>L<sub>in</sub></b>	<b>0</b> $\pm$ 4	<b>0</b> $\pm$ 4	-5 $\pm$ 3	<b>0</b> $\pm$ 4	-2 $\pm$ 3	-5 $\pm$ 3	-1 $\pm$ 3	-2 $\pm$ 2
<b>Q<sub>H</sub></b>	-86 $\pm$ 32	-96 $\pm$ 19	-36 $\pm$ 28	-68 $\pm$ 13	<b>-17</b> $\pm$ 28	-59 $\pm$ 27	-77 $\pm$ 14	-44 $\pm$ 23
<b>Q<sub>L</sub></b>	-194 $\pm$ 237	-126 $\pm$ 78	41 $\pm$ 150	-70 $\pm$ 83	<b>2</b> $\pm$ 140	5 $\pm$ 195	-5 $\pm$ 137	-24 $\pm$ 151
<b>Q<sub>M</sub></b>	-6 $\pm$ 9	-13 $\pm$ 9	<b>-4</b> $\pm$ 26	-32 $\pm$ 29	-6 $\pm$ 25	-9 $\pm$ 19	-28 $\pm$ 28	-14 $\pm$ 19

## Supplementary References

- Abrams, M., Crippen, R., and Fujisada, H. (2020). ASTER Global Digital Elevation Model (GDEM) and ASTER Global Water Body Dataset (ASTWBD). *Remote Sensing*, 12(7).
- Collins, W., Rasch, P., Boville, B., Hack, J., Mccaa, J., Williamson, D., and Kiehl, J. (2004). Description of the NCAR community atmosphere model (CAM 3.0). *NCAR Technical Note*, TN-464+STR.
- Dudhia, J. (1989). Numerical study of convection observed during the Winter Monsoon Experiment using a mesoscale two-dimensional model. *Journal of The Atmospheric Sciences*, 46:3077–3107.
- Farr, T. G., Rosen, P. A., Caro, E., Crippen, R., Duren, R., Hensley, S., Kobrick, M., Paller, M., Rodriguez, E., Roth, L., Seal, D., Shaffer, S., Shimada, J., Umland, J., Werner, M., Oskin, M., Burbank, D., and Alsdorf, D. (2007). The Shuttle Radar Topography Mission. *Reviews of Geophysics*, 45(2).
- Grell, G. A. (1993). Prognostic evaluation of assumptions used by cumulus parameterizations. *Monthly Weather Review*, 121(3):764 – 787.
- Grell, G. A. and Dévényi, D. (2002). A generalized approach to parameterizing convection combining ensemble and data assimilation techniques. *Geophysical Research Letters*, 29(14):38–1–38–4.
- Hong, S.-Y., Noh, Y., and Dudhia, J. (2006). A new vertical diffusion package with an explicit treatment of entrainment processes. *Monthly Weather Review*, 134(9):2318 – 2341.
- Iacono, M. J., Delamere, J. S., Mlawer, E. J., Shephard, M. W., Clough, S. A., and Collins, W. D. (2008). Radiative forcing by long-lived greenhouse gases: Calculations with the AER radiative transfer models. *Journal of Geophysical Research: Atmospheres*, 113(D13).
- Janjić, Z. I. (1994). The step-mountain eta coordinate model: Further developments of the convection, viscous sublayer, and turbulence closure schemes. *Monthly Weather Review*, 122(5):927 – 945.
- Janjić, Z. I. (1996). The surface layer in the NCEP eta model. In *Eleventh Conference on Numerical Weather Prediction, Norfolk, VA, 19-23 August, American Meteor Society, Boston, MA*, pages 345–355.
- Janjić, Z. I. (2002). Nonsingular implementation of the Mellor–Yamada Level 2.5 scheme in the NCEP meso model. *NCEP Office Note*, 436.
- Jiménez, P. A., Dudhia, J., González-Rouco, J. F., Navarro, J., Montávez, J. P., and García-Bustamante, E. (2012). A revised scheme for the WRF surface layer formulation. *Monthly Weather Review*, 140(3):898 – 918.
- Kain, J. S. (2004). The Kain-Fritsch convective parameterization: An update. *Journal of Applied Meteorology*, 43(1):170 – 181.
- Matsui, T., Zhang, S. Q., Lang, S. E., Tao, W.-K., Ichoku, C., and Peters-Lidard, C. D. (2018). Impact of radiation frequency, precipitation radiative forcing, and radiation column aggregation on convection-permitting West African monsoon simulations. *Climate Dynamics*, 55(1-2):193–213.
- Max, M.-D. C. and Suarez, M. J. (1994). An efficient thermal infrared radiation parameterization for use in general circulation models. *NASA Technical Memorandum*, 3(104606):85.
- Mesinger, F. (1993). Forecasting upper tropospheric turbulence within the framework of the Mellor-Yamada 2.5 closure. In *Res. Activ. in Atmos. and Ocean. Mod., WMO, Geneva, CAS/JSC WGNE*, volume 18, pages 4.28–4.29.
- Mlawer, E. J., Taubman, S. J., Brown, P. D., Iacono, M. J., and Clough, S. A. (1997). Radiative transfer for inhomogeneous atmospheres: RRTM, a validated correlated-k model for the longwave. *Journal of Geophysical Research: Atmospheres*, 102(D14):16663–16682.
- Monin, A. S. and Obukhov, A. M. (1954). Basic laws of turbulent mixing in the surface layer of the atmosphere. *Contrib. Geophys. Inst. Acad. Sci. USSR*, 24:163–187.

- Morrison, H., Thompson, G., and Tatarskii, V. (2009). Impact of cloud microphysics on the development of trailing stratiform precipitation in a simulated squall line: Comparison of one- and two-moment schemes. *Monthly Weather Review*, 137(3):991 – 1007.
- Nakanishi, M. and Niino, H. (2006). An improved Mellor–Yamada Level-3 model: Its numerical stability and application to a regional prediction of advection fog. *Boundary-Layer Meteorology*, 119:397–407.
- Nakanishi, M. and Niino, H. (2009). Development of an improved turbulence closure model for the atmospheric boundary layer. *Journal of the Meteorological Society of Japan. Ser. II*, 87(5):895–912.
- NASA Jet Propulsion Laboratory (JPL (2013). Shuttle Radar Topography Mission (SRTM) 1 Arc-Second Global [Data set]. NASA Earth Data. Accessed on August 1, 2020.
- NASA/METI/AIST/Japan Spacesystems and U.S./Japan ASTER Science Team (2019). ASTER Global Digital Elevation Model V003 [Data set]. NASA EOSDIS Land Processes DAAC. Accessed on August 1, 2020.
- Olson, J. B., Kenyon, J. S., Angevine, W. A., Brown, J. M., and Pagowski, Mariusz and Sušelj, K. (2019). A description of the MYNN-EDMF Scheme and the coupling to other components in WRF–ARW. *OAA Technical Memorandum OAR GSD*, 61:37.
- RGI Consortium (2017). Randolph glacier inventory – A dataset of global glacier outlines, version 6. NSIDC: National Snow and Ice Data Center. Accessed on May 01, 2022.
- Tewari, M., Chen, F., Wang, W., Dudhia, J., Lemone, A., Mitchell, E., Ek, M., Gayno, G., Wegiel, W., and Cuenca, R. H. (2004). Implementation and verification of the united N land surface model in the WRF model. In *20th Conference on Weather Analysis and Forecasting/16th Conference on Numerical Weather Prediction*, pages 11–15.